Electronic Supplementary Material (ESI) for Dalton Transactions.

Electronic Supplementary Information (ESI)

# Tetracyanidoferrate(–II) as Carbonyl Copycat

Franziska Jach,*[‡a,b] Theresa Block,[c] Yurii Prots,[a] Marcus Schmidt,[a] Matej Bobnar,[§a] Rainer Pöttgen,[c] Michael Ruck[a,b] and Peter Höhn[a]

a) Max-Planck-Institute for Chemical Physics of Solids, Nöthnitzer Strasse 40, 01187 Dresden, Germany. E-mail: Franziska.Jach@tu-dresden.de.

b) Faculty of Chemistry and Food Chemistry, Technische Universität Dresden, 01062 Dresden, Germany.

c) Institut für Anorganische und Analytische Chemie, Westfälische Wilhelms-Universität Münster, Corrensstraße 30, 48149 Münster, Germany.

‡ Current address: Fraunhofer Institute for Integrated Systems and Device Technology IISB, Schottkystraße 10, 91058 Erlangen, Germany

§ Current address: J. Stefan Institute, Jamova 39, 1000 Ljubljana, Slovenia.

## Content

## Experimental Procedures

### Synthesis

In view of the sensitivity of the starting materials and the reaction products to moisture and air, all manipulations associated with sample preparation and handling were performed in inert atmosphere using an argon-filled (Praxair, >99.999 %, purified with AirLiquide Oxisorb catalyst) glove box (MBraun, $p(O_2)/p^0 < 1$ ppm, $p(H_2O)/p^0 < 1$ ppm). $Sr_2N$ was synthesized from strontium (Alfa Aesar, distilled dendritic pieces, > 99.95 %) and nitrogen (Praxair, 99.999 %, further purified with molecular sieve, 3 Å, Merck) at 920 K. For the bulk synthesis of $(Sr_3N)_2[Fe(CN)_4]$, 0.5 g of a finely ground mixture containing $Sr_2N$, iron powder (Alfa Aesar, 99.998 %), graphite powder (Chempur, 99.9 %), and $NaN_3$ powder (Sigma Aldrich, 99.5 %) in the molar ratio Sr:Fe:C:N = 6:1:4:6 was pelletized, sealed in a tantalum ampoule in an argon atmosphere, placed in a silica Schlenk tube, and annealed at 1070 K for 24 h in Ar. Single crystals of $(Sr_3N)_2[Fe(CN)_4]$ were obtained from a mixture of $Sr_2N$, iron, graphite, and $NaN_3$ in a sodium flux. The nitrogen deficient reaction mixture contained the compounds in the molar ratio Sr:Fe:C:N = 6:1:4:5 (to prevent byproducts such as $SrCN_2$),[1] upon addition of an excess of metallic Na (to enhance crystallization) in an iron ampoule. After sealing, the iron ampoule was placed in an evacuated silica tube, heated to 1020 K with a rate of 100 K/h and annealed for 5 h, followed by slow cooling to room temperature with a rate of 1 K/h. After opening the iron ampoule, sodium was removed by distillation at 570 K and $10^{-3}$ mbar for 4.5 h.

## Chemical analysis

For the determination of the Sr, Fe, Ta, and Na contents, the ICP-OES technique was performed (Agilent Technologies ICP-OES 5100 Dual View); N, C, O, and H were analyzed via carrier-gas hot-extraction (LECO analyzer C-200 (carbon) and TCH-600 (other atoms)). For determination of the nitrogen content, powder samples were mixed with $KMnO_4$ in a mass ratio of 1:5. Calculated / observed (weight-%): Sr 74/68(1), Fe 7.8/8.2(3), C 6.7/7.4(4), N 11.77/13.34(1), contaminations Na 2.54(6), Ta ca. 0.02, O <0.25, H <0.02.

## Thermal analysis

Thermogravimetric (TG) measurements were carried out on a STA 449 C Jupiter F1 device by Netzsch. Powder samples were placed in open Ta crucibles and heated in Ar atmosphere. For differencial scannning calorimetry experiments samples were sealed in Ta ampoules, and the device DSC 404C Pegasus (Netzsch) was used. Samples were heated and cooled with a rate of 10 K/min, respectively. DSC signals were characterized by their maxima.

## IR- and Raman spectroscopy

Raman spectra of small crystallites were collected at room temperature using a Jobin-Yvon-Horiba LabRam spectrometer with an integrated Olympus BX40 microscope equipped with an Ar ion laser (514.532 nm). The spectral resolution was about 1.5 $cm^{-1}$. The finely ground (100 µm) powder samples were sealed in silica tubes with 1 mm diameter. If possible, the laser was focused on phase pure crystallites to exclude signals from impurities. Infrared spectra of finely ground powder samples were recorded in attenuated total reflectance (ATR) mode using a PerkinElmer UATR-Two FTIR spectrometer (spectral range 4000−450 $cm^{-1}$) inside the glove box. No signals indicating moisture in the samples have been detected by IR or Raman spectroscopy.

## Physical properties

Temperature-dependent electrical resistivity data was recorded using the 4-point Van-der-Pauw method while pressing the powder sample in a pressure cell at 2 kbar. Remaining elemental sodium was removed from the powder samples prior to measurement by distillation at 570 K and $10^{-3}$ mbar for 3 h.

## Mössbauer spectroscopy

A $^{57}Co/Rh$ source was used for the $^{57}Fe$ Mössbauer spectroscopic investigations of $(Sr_3N)_2[Fe(CN)_4]$. The sample was placed in a thin walled PMMA container with a diameter of 2 cm and an optimized thickness corresponding to Long *et al*.[2] The measurements were performed in usual transmission geometry at 293 and 78 K in a commercial bath cryostat while the source was kept at room temperature. The WinNormos for Igor program package was used for fitting the spectra.[3]

# Thermal Analysis

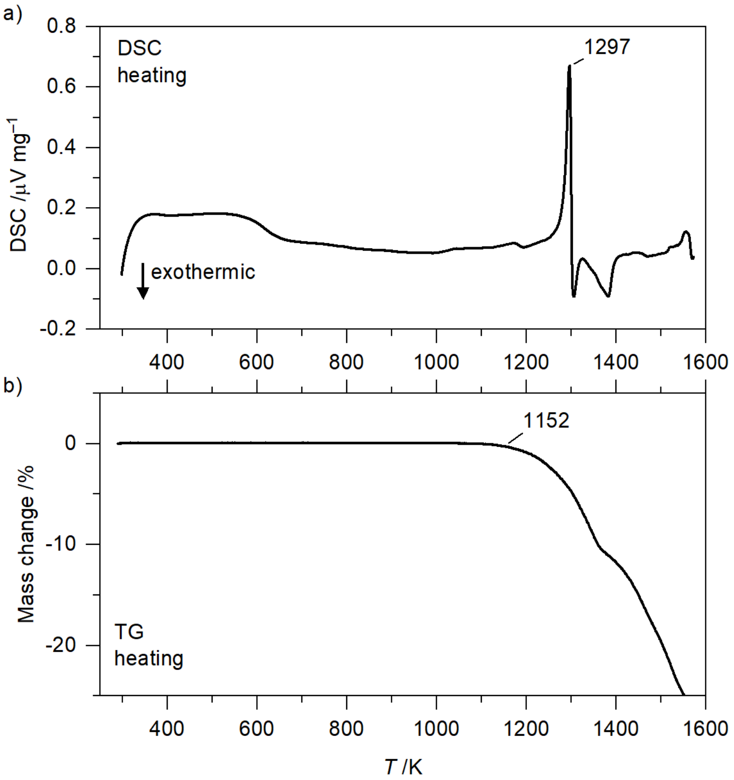

**Fig. S1** Thermal analysis of $(Sr_3N)_2[Fe(CN)_4]$ powder samples between 295 and 1573 K. a) Differential scanning calorimetry (DSC) in a closed Ta ampoule. b) Thermogravimetry (TG) in an open Ta crucible. No signals indicating the transformation of $(Sr_3N)_2[Fe(CN)_4]$ to $Sr_{3.5}[Fe(CN)_3]$[4] were observed by thermal analysis, most probably due to kinetic hindrace during fast heating. The transformation to $Sr_{3.5}[Fe(CN)_3]$ was observed during annealing experiments above 970 K for 24 h. The DSC signals at 1297, as well as the mass loss of ca. 25 % above 1150 K indicate the decomposition of the cyanoferrate structures. Decomposition products include $SrC_2$,[5] β-$SrCN_2$,[6] and $(Sr_6N)(FeN_2)(CN_2)_2$[7] amongst others according to powder X-ray diffraction.

## X-ray structure determination

Small transparent yellow hexagonal plate-like single crystals of $(Sr_3N)_2[Fe(CN)_4]$ were isolated from the bulk under dried paraffin oil by mechanical fragmentation and sealed in thin walled glass capillaries in argon atmosphere. X-ray diffraction data were collected on a Bruker APEX II Kappa CCD four-circle diffractometer, equipped with Mo-$K_\alpha$ radiation and graphite monochromator. The structure in *R*3*c* was solved and refined using the charge flipping algorithm and the Jana2006 program package.[8] The crystal shows obverse/reverse twinning, each completed with inversion domains.

Cell parameters were determined by Rietveld refinement against synchrotron powder diffraction data. The data were measured at beamline BL04-MSPD, ALBA Barcelona (Spain). Finely ground powders were sealed in thin walled glass capillaries. The space group and structural model derived from single crystal data is verified by good agreement to experimental powder data. The powder data indicates contamination of the bulk sample with small amounts of $Sr_4N[C_2N][CN_2]$,[9] elemental Fe and further unknown phases.

### Crystallographic data for $(Sr_3N)_2[Fe(CN)_4]$

Trigonal; space group *R*3c (no. 161); $a = 702.12(2)$ pm, $c = 4155.5(2)$ pm, $V = 1774.1(1)\ 10^6$ pm$^3$; $Z = 6$; $\rho_{calc} = 4.01$ g cm$^{-3}$; Single crystal X-ray diffraction: $\lambda = 71.073$ pm (Mo-$K_\alpha$); $T = 293(1)$ K; $2\theta_{max} = 70.2°$; $-11 \leq h \leq 11$, $-11 \leq k \leq 11$, $-66 \leq l \leq 66$; 39012 measured, 2896 unique reflections; $\mu = 28.02$ mm$^{-1}$; Twin fractions 100010001 (0.52(2)) −1000−10001 (0.14(1)) −1000−1000−1 (0.33(2)) 10001000−1 (0.01(1)); $R_{int} = 0.077$, $R_\sigma = 0.041$, 57 parameters, $R_1(2387\ F_o > 3\sigma(F_o)) = 0.043$, $wR_2(\text{all } F_o) = 0.067$, *GOF* = 2.50, min./max. residual electron density: −1.23/1.90 *e* $10^{-6}$ pm$^{-3}$. For atomic parameters including applied restraints and constraints due to stacking faults see Tables S1, S2, for interatomic distances see Table S3. Rietveld refinement against synchrotron powder diffraction data: $\lambda = 32.641(1)$ pm, $T = 293(1)$ K, $2.304° \leq 2\theta \leq 17.865°$, Structural parameters 12, $wR_{Profile} = 0.231$, $wR_{Bragg}$ (all $F_o$) = 0.116, *GOF* = 1.31, min./max. residual electron density: −2.93/2.61 *e* $10^{-6}$ pm$^{-3}$. Small regions showing overlapping reflections of known ($Sr_4N[C_2N][CN_2]$, Fe) and unknown impurity phases were excluded from refinement. Regarding $(Sr_3N)_2[Fe(CN)_4]$, atomic positions of Sr and Fe were further refined, while parameters of C and N were kept constant. For a plot of the Rietveld fit see Figure S2. Given distances were calculated using the cell parameters from powder refinement and atomic positions according to single crystal data. Further details of the crystal structure determination are provided free of charge by the joint Cambridge Crystallographic Data Centre and Fachinformationszentrum Karlsruhe by quoting the repository number (CSD-2127618). Access Structure via www.ccdc.cam.ac.uk/structures.

**Table S1** Atom sites and isotropic / equivalent displacement factors for $(\mathrm{Sr_3N})_2[\mathrm{Fe(CN)_4}]$ according to X-ray single crystal refinement. Atom sites labelled “a” correspond to the ideal ordered structure, while sites labelled “b” and “c” correspond to stacking faults observed in the structure.

The following restraints and constraints were applied: Positions: x, y coordinates were kept equal for “a”, “b”, “c” positions, while z coordinates are shifted, realized by fixed distances. Example: (x’,y’)[Sr2b] = (x,y)[Sr2a]; *d*(Sr2a–Sr2b) = *d*(Sr2b–S2c) = ⅓ *c* and *d*(Sr2a–Sr2c) = ⅔ *c*. Occupancies: occupancies of “a”, “b”, “c” positions sum up to 1. Example: *occ*[Sr2a] + *occ*[Sr2b] + *occ*[Sr2c] = 1. Thermal displacement parameters were kept equal for “a”, “b”, “c” positions. Example: *U*[Sr2a] = *U*[Sr2b] = *U*[Sr2c]. Carbon and nitrogen positions were refined with isotropic displacement parameters.

| Atom | Site | Occupancy | *x* / *a* | *y* / *b* | *z* / *c* | $U_{\mathrm{iso}}$, $U_{\mathrm{eq}}$ / Å$^2$ |
|---|---|---|---|---|---|---|
| Sr1 | 18*b* | 1 | 0.3110(1) | 0.9823(2) | 0.93337(2) | 0.0107(3) |
| Sr2a | 18*b* | 0.889(2) | 0.6658(1) | 0.9279(1) | 0.86179(2) | 0.0077(2) |
| Fe1a | 6*a* | 0.874(4) | 0 | 0 | 0.00017(4) | 0.0048(4) |
| C1a | 6*a* | 0.881 | 0 | 0 | 0.0453(3) | 0.005(2) |
| C2a | 18*b* | 0.881 | 0.758(1) | 0.002(1) | 0.9849(2) | 0.008(1) |
| N1a | 6*a* | 0.881 | ⅔ | ⅓ | 0.9079(3) | 0.017(2) |
| N2a | 18*b* | 0.881 | 0.602(1) | 0.001(1) | 0.9726(2) | 0.019(1) |
| N3ac | 6*a* | 0.911 | 0 | 0 | 0.8955(2) | 0.007(1) |
| N3ab | 6*a* | 0.97 | 0 | 0 | 0.2288(2) | 0.007(1) |
| N3bc | 6*a* | 0.119 | 0 | 0 | 0.5622(2) | 0.007(1) |
| Sr2b | 18*b* | 0.081(6) | 0.6658 | 0.9279 | 0.19512(2) | 0.0077 |
| Fe1b | 6*a* | 0.086(7) | 0 | 0 | 0.33350(4) | 0.0048 |
| C1b | 6*a* | 0.089 | 0 | 0 | 0.3786(3) | 0.005 |
| C2b | 18*b* | 0.089 | 0.758 | 0.002 | 0.3183(2) | 0.008 |
| N1b | 6*a* | 0.089 | ⅔ | ⅓ | 0.2412(3) | 0.017 |
| N2b | 18*b* | 0.089 | 0.602 | 0.001 | 0.3060(2) | 0.019 |
| Sr2c | 18*b* | 0.030(7) | 0.6658 | 0.9279 | 0.52845(2) | 0.0077 |
| Fe1c | 6*a* | 0.039(8) | 0 | 0 | 0.66683(4) | 0.0048 |
| C1c | 6*a* | 0.03 | 0 | 0 | 0.7119(3) | 0.005 |
| C2c | 18*b* | 0.03 | 0.758 | 0.002 | 0.6516(2) | 0.008 |
| N1c | 6*a* | 0.03 | ⅔ | ⅓ | 0.5745(3) | 0.017 |
| N2c | 18*b* | 0.03 | 0.602 | 0.001 | 0.6393(2) | 0.019 |

**Table S2** Anisotropic displacement factors $U_{\mathrm{ij}}$ /Å$^2$ of $(\mathrm{Sr_3N})_2[\mathrm{Fe(CN)_4}]$ according to X-ray single crystal refinement. The $U_{\mathrm{ij}}$ factors of the atomic positions Sr2a, Sr2b, Sr2c as well as Fe1a, Fe1b, Fe1c were restricted to be equal.

| Atom | $U_{11}$ | $U_{22}$ | $U_{33}$ | $U_{12}$ | $U_{13}$ | $U_{23}$ |
|---|---|---|---|---|---|---|
| Sr1 | 0.0122(4) | 0.0120(4) | 0.0086(3) | 0.0065(2) | −0.0006(2) | 0.0002(2) |
| Sr2a | 0.0058(2) | 0.0081(3) | 0.0087(3) | 0.0030(2) | 0.0000(2) | 0.0023(2) |
| Fe1a | 0.0055(4) | 0.0055(4) | 0.0034(7) | 0.0027(2) | 0 | 0 |

**Table S3** Selected interatomic distances /pm and angles /°. With an exception of the tetrahedral anion $[Fe(CN)_4]^{6-}$, shortest distances between two atom types are shown, respectively. For calculation of the distances cell parameters according to Rietveld refinement and atomic coordinates according to single crystal refinement (see above) were used.

| Atoms | Distance | Atoms | Distance | Atoms | Angles |
|---|---|---|---|---|---|
| Fe1a–C1a | 187(1) | Sr···N | 238.5(8) | Fe1a–C1a–N1a | 180 |
| Fe1a–C2a | 183(1) | Sr···C | 291.0(7) | Fe1a–C2a–N2a | 175.1(7) |
| C1a–N1a | 122(2) | Sr···Fe | 307.7(1) | C1a–Fe1a–C2a | 110.3(2) |
| C2a–N2a | 120(1) | Sr···Sr | 342.5(1) | C2a–Fe1a–C2a | 108.6(4) |
| | | Fe···Fe | 702.12(2) | | |

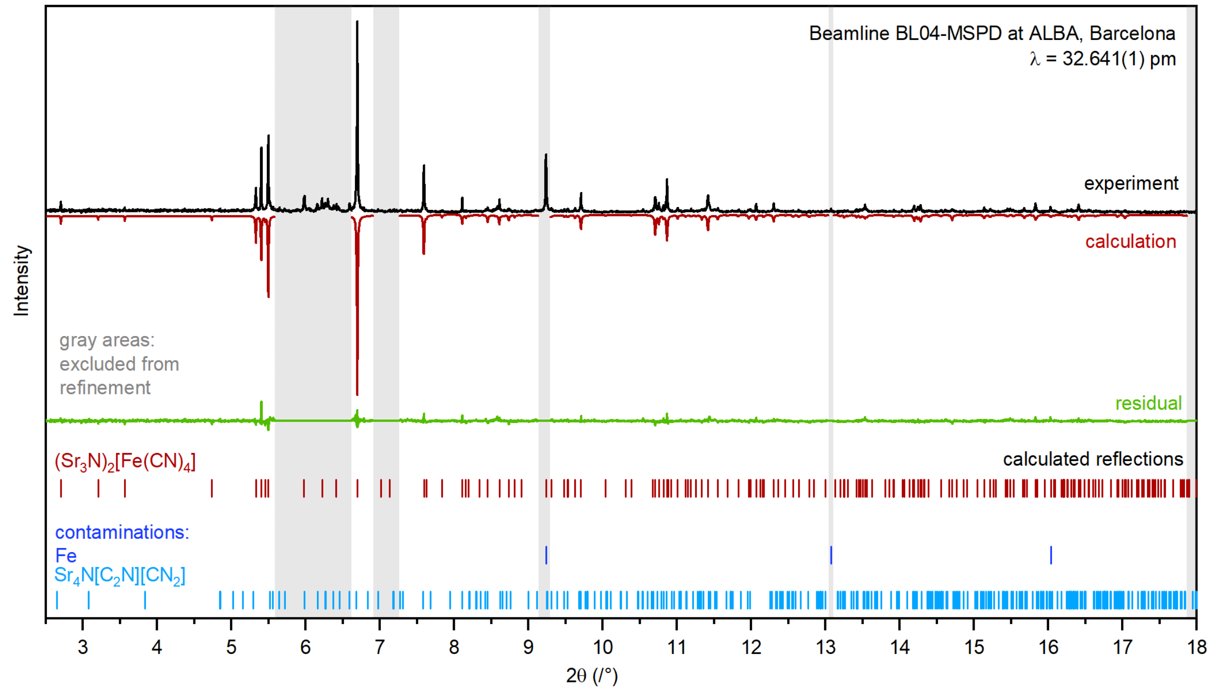

**Fig. S2** Rietveld refinement of $(Sr_3N)_2[Fe(CN)_4]$ against synchrotron powder diffraction data. The data confirms the space group symmetry, since only reflections agreeing to a *R*-centered cell were observed (space group *R*3*c*). Regions excluded from refinement due to overlapping with reflections of known ($Sr_4N[C_2N][CN_2]$, Fe) and unknown impurity phases are marked as gray areas.

## Stacking faults and disordered structural model

Diffuse scattering along *c** in diffraction layers (Figure S3) hints towards stacking faults along *c*. Refining an ordered structural model with main atomic positions (labelled "a") only yields additional electron density peaks in the $F_{diff}$ map (Figure S4), which can as well be interpreted as faulty stacked layers.

Thus, these stacking faults were included during further refinement of single crystal diffraction data using a disordered structural model: Besides the main atom positions (labelled "a") corresponding to the ideal ordered structure, further minor positions were introduced representing shifted main positions. Positions labelled "b" thereby correspond to a shift of 1/3 along [001] of the main "a" position, while "c" positions are shifted by 2/3 along [001] with respect to "a" positions. This is equivalent to a shift of "b" and "c" domains along [1−10] with respect to "a": complete layers shifted within the *ab* plane, i.e. faulty stacked layers. The thus developed disordered model yields overlapping positions for carbon and nitrogen atoms and was therefore stabilized using constraints and restraints (Table S1). The atomic position Sr1 was handled using anisotropic displacement parameters instead of shifted positions due to its coordinates close to (1/3,1/3,z) which yield only minor changes during shifting along [1−10].

Occupancy values of the atomic positions Sr2a and Fe1a, were not constrained with respect to each other and refined as independent variables. Corresponding minor positions Sr2b/Fe1b, and Sr2c/Fe1c were handled similarly. For all domains “a”, “b”, “c”, refined occupancy values *occ* yield similar results for Sr and Fe positions: $occ_a$ (Sr2a/Fe1a) = 0.889(2)/0.874(4), $occ_b$ (Sr2b/Fe1b) = 0.081(6)/0.086(7), $occ_c$ (Sr2c/Fe1c) = 0.030(7)/0.039(8). These results allow to conclude that the minor positions Sr2b/Fe1b and Sr2c/Fe1c indeed belong to two additional domains representing whole layers of the original structure shifted by 1/3 (for “b”), and by 2/3 (for “c”) in [1−10] direction in comparison to main domain positions “a”. In contrast, a local disorder of individual atomic positions would not yield similar occupancies for Sr2a/Fe1a and Sr2b/Fe1b.

The occupancy values of nitrogen and carbon positions were defined and fixed according to the values of Sr2a and Fe1a that were refined before. Nitrogen positions N3ac, N3ab, N3bc centered in $Sr_6$ octahedra represent mixtures of main (“a”) and minor (“b”, “c”) domains because in each domain two of these atomic positions occur. Therefore, their occupancies sum up to 2 in total, and are each defined and fixed as a sum of the corresponding two domains.

In comparison to an ordered structural model taking into account only main positions “a”, the resulting disordered structural model exhibits significantly better residuals and a lower residual electron density. In addition, the disordered model yields chemically reasonable C–N distances for both ligand positions: ordered model *d*(C1a–N1a/C2a–N2a) = 114(7)/124(4) pm, disordered model *d*(C1a–N1a/C2a–N2a) = 122(2)/120(1) pm. The similar C–N distances for both ligand types in the disordered model agrees well with the observed Raman spectrum showing only a small deviation of the split maxima of the strong v(CN) valence band (1690, 1706 $cm^{-1}$).

Summarizing, the crystal consists of three domains (“a”, “b”, “c”) which are fully ordered in stacking sequence ..ABCA’B’C’.. and are thus identical to each other within the domains. However, at some points of the structure, the main stacking sequence is interrupted by a faulty stacked layer. A new domain starts by a faulty shifted layer in [1–10] direction in comparison to the expected next layer of the original domain.

Stacking faults are most probable, if the local environment of the atoms, and thus, chemical bonding, does not change. In the main stacking sequence of the current structure, the positions of tetracyanidoferrate anions shift in [1–10] direction and are turned along [001] from layer to layer. Therefore, a domain change from “a” to “b” (e.g. A→C’) in [001] direction is more likely to happen than from “a” to “c” (A→A’). In the latter case, $[Fe(CN)_4]^{6-}$ anions would be stacked above one another in adjacent layers (see Fig. S5a), resulting in a dramatic change in chemical environment compared to the main stacking sequence. These considerations yield a probable domain stacking sequence of “a”→“b”→“c”→“a” as depicted in Fig. S5b for this structure, with fractions of the domains being 88 % “a”, 9 % “b”, and 3 % “c”. The layer stacking sequence ABCA’B’C’ is only slightly disturbed by the domains, since stacking faults occur only at domain boundaries.

Furthermore, the building faults observed in the structure might be the reason for the small amount of observed reflections in the data set not compatible with obverse/reverse twinning.

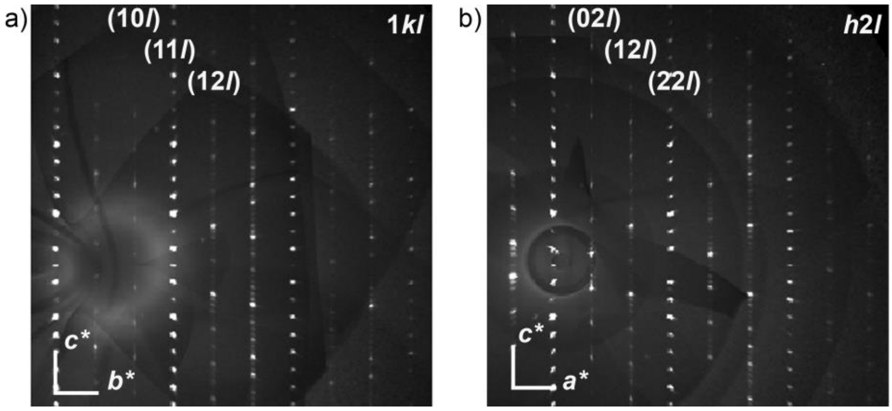

**Fig. S3** Diffraction layers displaying diffuse scattering along c*. a) 1*kl*. b) *h*2*l*.

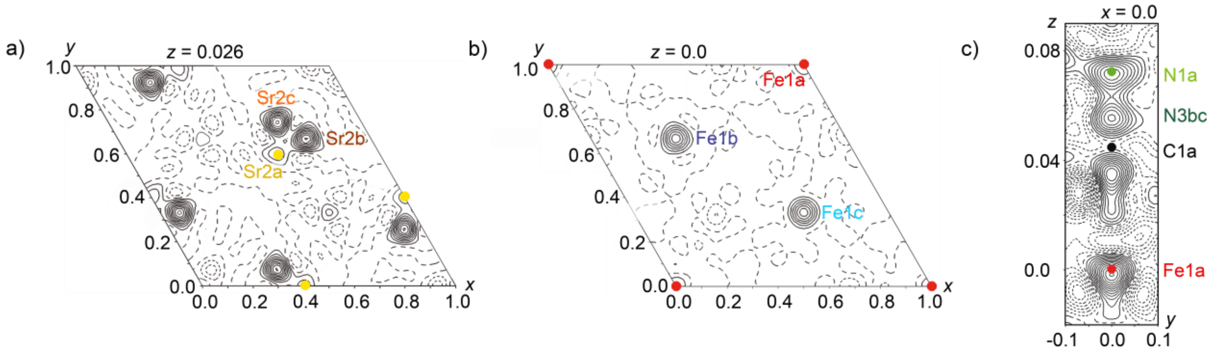

**Fig. S4** Refinement as an ordered structure (with “a” positions only) yields additional electron density peaks in the $F_{\text{diff}}$ maps. Main atomic positions (“a”) are denoted as coloured spheres. Electron density peaks are labelled according to minor positions (“b”, “c”) included in the disordered structural model. a) View of Sr2 positions at $z$ = 0.026. b) View of Fe1 positions at $z$ = 0. c) View of C1N1 ligand at $x$ = 0.

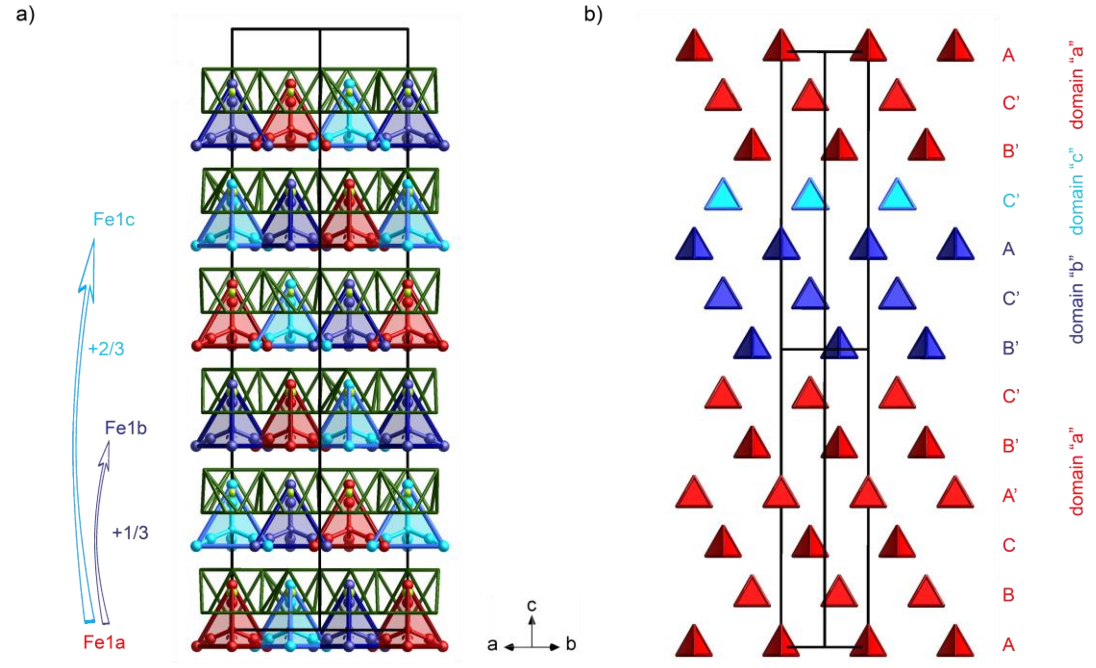

**Fig. S5** Development and refinement of the disordered model. a) Development of additional domains “b” and “c” for $[Fe(CN)_4]^{6-}$ tetrahedra as a representative example. All positions are shifted with respect to domain “a” by $z$ + ⅓ and $z$ + ⅔ for “b” and “c”, respectively. $[Fe1a(CN)_4]^{6-}$ tetrahedra are drawn in red, Fe1b tetrahedra dark blue, Fe1c tetrahedra light blue. For simplicity reasons, only parts of the structure are shown and all tetrahedral atoms (Fe, C, N) are depicted same-coloured. View in [−1−10] direction. b) Sketch of possible domains and stacking sequences of the disordered structure. For simplicity reasons, only $[Fe(CN)_4]^{6-}$ tetrahedra along the diagonal in [1−10] direction are shown.

# IR- and Raman spectroscopy

**Table S4.** Expected internal vibrational modes for the $[Fe(CN)_4]^{6-}$ anion within the $(Sr_3N)_2[Fe(CN)_4]$ solid state structure according to molecular site group analysis,[10,11] including vibrational symmetry types and the assignment to experimentally observed bands in IR and Raman (R) spectrum. For the assignment of symmetry types to molecular vibrations of the isolated molecule, spectroscopic data of the isoelectronic, tetrahedrally coordinated $[Fe(CO)_4]^{2-}$ anion were used as reference.[10,12] To allow a clearer comparison of expectations to experimental data, vibrational modes are sorted by molecular vibration instead of symmetry type.

| *Mecke* notation/ Molecular vibration | Molecular point group | Molecular selection rules | Site symmetry | Factor group | Solid state selection rules | Observed bands /cm$^{-1}$ | |
|---|---|---|---|---|---|---|---|
| | $T_d$ | | $C_3$ | $C_{3v}$ | | IR | R |
| $\nu(CN) = \nu_1$ | $A_1$ | R | $A$ | $A_1$ | IR, R | | 1706 |
| | | | | $A_2$ | – | | |
| $\nu(CN) = \nu_6$ | $F_2$ | IR, R | $A$ | $A_1$ | IR, R | 1688 | 1690 |
| | | | | $A_2$ | – | | |
| | | | $E$ | $E$ | IR, R | | |
| $\nu(FeC) = \nu_2$ | $A_1$ | R | $A$ | $A_1$ | IR, R | | |
| | | | | $A_2$ | – | | |
| $\nu(FeC) = \nu_7$ | $F_2$ | IR, R | $A$ | $A_1$ | IR, R | | |
| | | | | $A_2$ | – | | |
| | | | $E$ | $E$ | IR, R | | |
| $\delta(FeCN) = \nu_3$ | $E$ | R | $E$ | $E$ | IR, R | } 482, 527, 543, 582 | 415, 472, 529, 543, 584, 594, 619 |
| $\delta(FeCN) = \nu_5$ | $F_1$ | – | $A$ | $A_1$ | IR, R | | |
| | | | | $A_2$ | – | | |
| | | | $E$ | $E$ | IR, R | | |
| $\delta(FeCN) = \nu_8$ | $F_2$ | IR, R | $A$ | $A_1$ | IR, R | | |
| | | | | $A_2$ | – | | |
| | | | $E$ | $E$ | IR, R | | |
| $\delta(CFeC) = \nu_4$ | $E$ | R | $E$ | $E$ | IR, R | | } < 270 |
| $\delta(CFeC) = \nu_9$ | $F_2$ | IR, R | $A$ | $A_1$ | IR, R | | |
| | | | | $A_2$ | – | | |
| | | | $E$ | $E$ | IR, R | | |

# References

[1] U. Berger, W. Schnick, *J. Alloys Compd.*, 1994, **206**, 179-184.

[2] G. J. Long, T. Cranshaw, G. Longworth, *Mössbauer Eff. Ref. Data J.*, 1983, **6**, 42-49.

[3] R. A. Brand*, WinNormos for Igor6* (version for Igor 6.2 or above: 22.02.2017), Universität Duisburg, Duisburg, Germany, 2017**.**

[4] F. Jach, F. R. Wagner, Z. H. Amber, M. Rüsing, J. Hunger, Yu. Prots, M. Kaiser, M. Bobnar, A. Jesche, L. M. Eng, M. Ruck, P. Höhn, *Angew. Chem.*, 2021, **133**, 16015-16021; *Angew. Chem. Int. Ed.*, 2021, **60**, 15879-15885.

[5] V. Vohn, M. Knapp, U. Ruschewitz, *J. Solid State Chem.*, 2000, **151**, 111-116.

[6] W. Liao, R. Dronskowski, *Acta Crystallogr., Sect. E: Struct. Rep. Online*, 2004, **60**, i124-i126.

[7] J. K. Bendyna, P. Hoehn, R. Kniep, *Z. Kristallogr. - New Cryst. Struct.*, 2009, **224**, 5-6.

[8] V. Petříček, V.; Dušek, M.; Palatinus, L., *Z. Kristallogr.*, 2014, **229**, 345-352.

[9] F. Jach, P. Höhn, Yu. Prots, M. Ruck, *Eur. J. Inorg. Chem.*, **2019**, 1207-1211.

[10] J. Weidlein, U. Müller, K. Dehnicke, *Schwingungsspektroskopie*, Thieme, Stuttgart, 1988.

[11] D. L. Rousseau, R. P. Bauman, S. P. S. Porto, *J. Raman Spectrosc.*, 1981, **10**, 253-290.

[12] H. Stammreich, K. Kawai, Y. Tavares, P. Krumholz, J. Behmoiras, S. Bril, *J. Chem. Phys.*, 1960, **32**, 1482-1487.